nature nanotechnology

LETTERS

PUBLISHED ONLINE: 14 DECEMBER 2008 | DOI: 10.1038/NNANO.2008.363

Imaging the electrical conductance of individual carbon nanotubes with photothermal current microscopy

Adam W. Tsen[1], Luke A. K. Donev[2], Huseyin Kurt[3], Lihong H. Herman[1] and Jiwoong Park[4]*

The one-dimensional structure of carbon nanotubes[1] leads to a variety of remarkable optical[2] and electrical[3] properties that could be used to develop novel devices[4]. Recently, the electrical conductance of nanotubes has been shown to decrease under optically induced heating by an amount proportional to the temperature change[5]. Here, we show that this decrease is also proportional to the initial nanotube conductance, and make use of this effect to develop a new electrical characterization tool for nanotubes. By scanning the focal spot of a laser across the surface of a device through which current is simultaneously measured, we can construct spatially resolved conductance images of both single and arrayed nanotube transistors. We can also directly image the gate control of these devices. Our results establish photothermal current microscopy as an important addition to the existing suite of characterization techniques for carbon nanotubes and other linear nanostructures.

Scanning photocurrent (SPC) measurements have been used to image the electronic band mapping of carbon nanotube transistors[6–9]. Although the photocurrent exhibits strong gate-dependence, it is not a direct probe of device conductance because a photocurrent is also generated when the nanotube is turned 'off'. In contrast, the conductance of nanotubes is directly susceptible to changes in temperature[10,11]. In this paper, we induce local heating of nanotube devices under applied bias using a setup similar to that used in SPC measurements (Fig. 1a). We first develop an understanding of the relationship between the heat-induced current signal and the overall electrical conductance of the device for both metallic and semiconducting nanotubes, and then make use of this relation to image the gate-dependent conductance of various nanotube devices.

On the left in Fig. 1b, we show an atomic force microscope (AFM) image of a representative device D1, a semi-metallic nanotube (diameter ~2.8 nm) contacted by two palladium/chromium/gold electrodes. When no bias is applied, strong photocurrent spots are observed in the current image at the nanotube–metal interfaces, as expected[6–9] (see Supplementary Information, Fig. S1). As the bias is increased, however, a new effect is observed within the nanotube bulk.

On the right in Fig. 1b, in false colour, we show a current image of D1 corresponding to $V_D > 0$, taken with heterodyne detection (see Methods). We can see a strong current signal along the entire length of the nanotube. The reflection image is overlaid, so that the electrodes (outlined with dashed lines) are visible, and the circuit used in the measurement is shown for reference. Because current is measured in an a.c. mode, the colour at each point in the image represents the change in current ΔI measured in the device when the laser is incident on it. Comparison with the AFM image then suggests that device current changes when the laser spot is positioned on the nanotube. In particular, the polarity of ΔI is always the same throughout the device, maintaining its direction opposite to that of the d.c. current. This effect is independent of bias polarity (see Supplementary Information, Fig. S2), strongly suggesting that the signal is due to a laser-induced conductance decrease in our nanotube device. Furthermore, this signal anywhere along the nanotube is found to scale linearly with V_D (Fig. 1c, left; measured with standard lock-in), indicating that the conductance change $\Delta G = \Delta I / V_D$ is the fundamental quantity of interest in our experiment.

This light-induced conductance change, which is the central finding of our experiment, cannot be explained by previously reported photoelectric effects in carbon nanotubes. Under applied bias both photocurrent[7]and photoconductivity[12] generate additional current in the same direction as the d.c. current, opposite to the signal in Fig. 1b. Furthermore, they cannot explain the conductance and gate-dependent behaviours of the current signal described later (Fig. 3).

From the anisotropic laser polarization dependence of the current signal (Fig. 1c, middle; $V_D = 0.2$ V, standard lock-in), we rule out mechanisms that originate from the exterior of the nanotube, such as photoelectric gating[12,13]. Meanwhile, the short timescale of the measurements makes the effect of molecular photodesorption[14] an unlikely cause of the conductance change (see Methods for further discussion of these effects).

One direct way that light absorption can reduce the conductance of a nanotube is by increasing its temperature[5]. Under applied bias, d.c. current flows continuously through the device. However, as the beam is scanned over the nanotube, a fraction of light power is absorbed and converted into heat, increasing the temperature of the nanotube. This then changes the device conductance by an amount ΔG and creates a current differential, or photothermal current $\Delta I = \Delta G \cdot V_D$. Because we expect ΔG to be negative, ΔI is negative (positive) for positive (negative) V_D, as is the case in Fig. 1c. In other words, the focused laser spot acts as a local heat source, and the nanotube device acts as a local temperature sensor. A schematic of this process is shown in the top panels of Fig. 1a.

We can relate the heat-induced conductance decrease ΔG to $G(T)$ as $\Delta G = (dG/dT)\Delta T$, where T and ΔT are, respectively, the temperature and temperature increase of the nanotube, averaged along the nanotube length. As we expect ΔT to scale linearly with irradiance for the light levels used in the experiment, we confirm this by measuring $|\Delta I|$ for D1 ($V_D = 0.2$ V, standard lock-in) as a

[1]Department of Applied Physics, Cornell University, Ithaca, New York 14853, USA, [2]Laboratory of Atomic and Solid-State Physics, Cornell University, Ithaca, New York 14853, USA, [3]The Rowland Institute at Harvard, Harvard University, Cambridge, Massachusetts 02142, USA, [4]Department of Chemistry and Chemical Biology, Cornell University, Ithaca, New York 14853, USA; *e-mail: jpark@cornell.edu

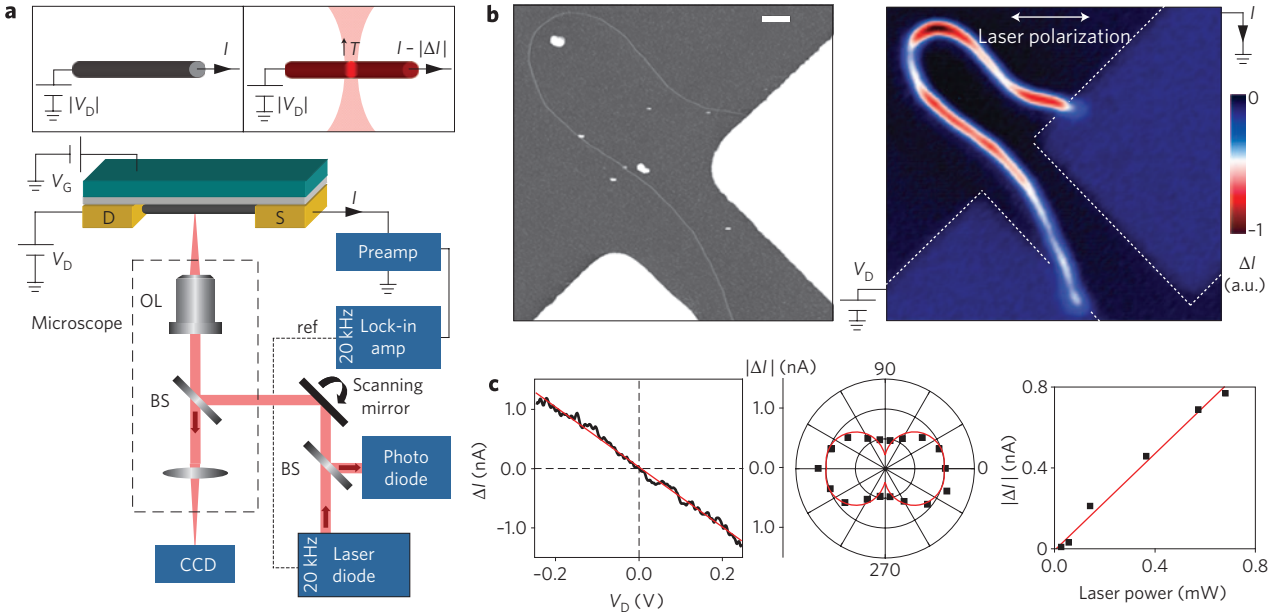

Figure 1 | Laser heating-induced decrease in conductance of an individual carbon nanotube transistor. a, Main panel: schematic of the scanning laser setup with simultaneous electrical measurement using a standard lock-in technique and the nanotube device studied. The laser beam is split by two beamsplitters (BS) and focused onto the nanotube through an objective lens (OL). The scanning mirror galvo rasters the focused beam across the surface of the sample. Electrical current through the device and reflected light intensity are recorded as a function of the position of the laser spot. A 20 kHz laser intensity modulation is used for the current signal. Top diagram showing mechanism of a.c. generation by laser heating. The laser increases the temperature of the nanotube and decreases device conductance and current. An alternative, heterodyne scheme is also used (Fig. 4a). **b**, Left: AFM image of the nanotube device D1 with diameter ~2.8 nm. Scale bar, 1 μm. Right: a.c. current image (PTCM) of D1 corresponding to $V_D > 0$ taken with heterodyne detection. Laser incidence on the nanotube induces a current change corresponding to a lowering of device conductance. The measurement circuit, electrodes and reflection image (overlaid) are shown for reference. **c**, Bias (left), polarization (middle) and laser power (right) dependence of current signal with the laser fixed on the nanotube. ΔI scales linearly with V_D and laser power in the measured range, and displays polarization anisotropic behaviour typical of light absorption. Laser-induced conductance decrease is independent of bias polarity.

function of laser power while fixing the laser on the nanotube (Fig. 1c, right).

The form of dG/dT can be deduced from the reported temperature dependence of the electrical conductivity of carbon nanotubes, which is inversely proportional to temperature T near room temperatures for both metallic[10] and semiconducting nanotubes in the 'on' state[11]. Therefore, we can represent the total resistance of our device as $R = R_{int}(T/T_{RT}) + R_C$, where R_{int} and R_C represent the intrinsic resistance of the carbon nanotube at room temperature and contact resistance (which is relatively insensitive to temperature[10]), respectively. From this, we derive $dG/dT = -(G/T_{RT})(R_{int}/R)$. When the intrinsic nanotube resistance is the dominant factor (small R_C), this becomes $dG/dT = -G/T_{RT}$, whereas in the opposite limit (large R_C), we obtain $dG/dT = -(G^2/T_{RT})R_{int}$. Based on this, we expect that ΔG will scale monotonically with G, with a power-law exponent between 1 and 2.

Our measurements support this scaling. In Fig. 2a, we show photothermal current microscopy (PTCM) images of three devices D2, D3 and D4 with different resistances taken at identical bias and laser conditions ($V_D = 0.2$ V, standard lock-in). The photothermal current is overall largest (smallest) for the most (least) conductive device, a behaviour that is universally observed. In addition to this general trend, we observe interesting spatial variation of the current signal in Fig. 2b, which we ascribe to surface-related effects and not intrinsic nanotube defects (see Supplementary Information, Fig. S3). In Fig. 2b (main panel), we plot $|\Delta G|$ (averaged along the nanotube length, standard lock-in) versus G in log–log scale for 11 nanotubes of length ~5 μm under ~1 mW laser illumination. All nanotubes shown here have relatively large diameters (1.5 to 5 nm) and show metallic or semi-metallic characteristics. We see that $|\Delta G|$ increases monotonically with G for over an order of magnitude, with the line of best fit revealing a power dependence of 1.46 ± 0.19, substantiating our prediction if we assume similar ΔT for these devices. From these data, we extract $\Delta T = 0.4$ K on average per 1 mW laser illumination for ~5-μm-long nanotubes (see Methods for further discussion). Here, optical absorption for the different nanotubes used in the experiment is assumed to be relatively uniform in the visible wavelengths, as supported by the measurements on five of the eleven nanotubes using equal-intensity lasers of wavelengths $\lambda = 410$ nm and 658 nm (Fig. 2b, inset).

Our knowledge of the average temperature increase allows us to further estimate the thermal resistance $R_{th} = \Delta T/P$ between the nanotube and the substrate, where P is the heat power loss through the interface. Using the measured absorption cross-section for single-walled carbon nanotubes[15], we calculate that a 2-nm-diameter nanotube will absorb ~75 nW of the 1 mW laser. Because nonradiative decay in carbon nanotubes has been measured to occur on a ~1 ps timescale[16], which is at least five orders of magnitude faster than that of radiative decay[17], we can assume that all of the absorbed light will be converted into heat. We then calculate $R_{th} = (0.4\ \text{K} \times 5\ \mu\text{m})/75\ \text{nW} \approx 25\ \text{m K W}^{-1}$ per unit length for a 2-nm-diameter nanotube, a value that is within an order of magnitude of previously reported values[18].

To the best of our knowledge, this is the first time that laser-induced heating of individual nanotubes has been studied quantitatively in conjunction with their electrical properties. By making use of the effect of heating on device conductance, we are able to image nanotube transistors quickly with submicrometre resolution and probe the conductance of the device simultaneously. Furthermore,

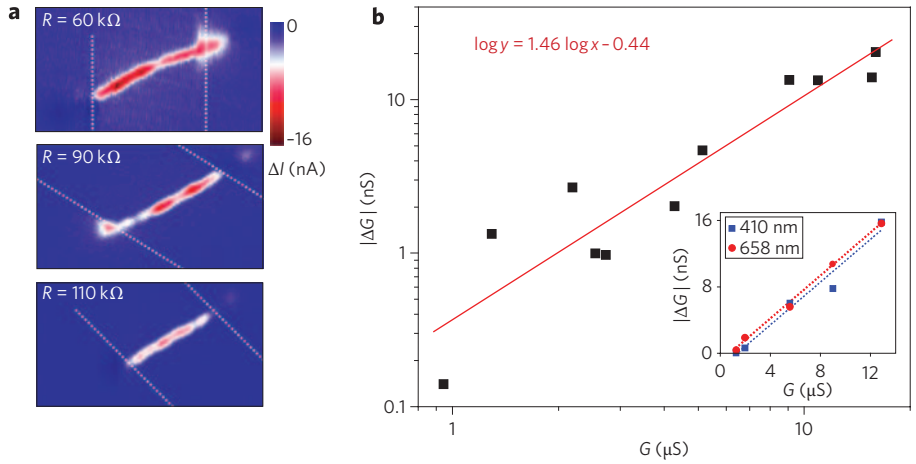

Figure 2 | Dependence of photothermal current on overall device conductance. a, PTCM images of carbon nanotube devices D2, D3 and D4 (resistances 60, 90 and 110 kΩ) with $V_D = 0.2$ V taken with standard lock-in. Electrode boundaries are marked with dotted lines. The overall signal is largest (smallest) for the most (least) conducting device. **b**, Main panel: magnitude of laser-induced conductance decrease $|\Delta G| = |\Delta I/V_D|$, averaged over the nanotube length, versus overall conductance G for 11 carbon nanotube devices in log–log scale. $|\Delta G|$ scales monotonically with G for over an order of magnitude. The line of best fit reveals a power dependence of 1.46 ± 0.19, in agreement with predicted heating behaviour. Inset: same plot for five devices using different laser wavelengths (410 nm, 658 nm, equal intensity) show similar heating behaviour for both wavelengths.

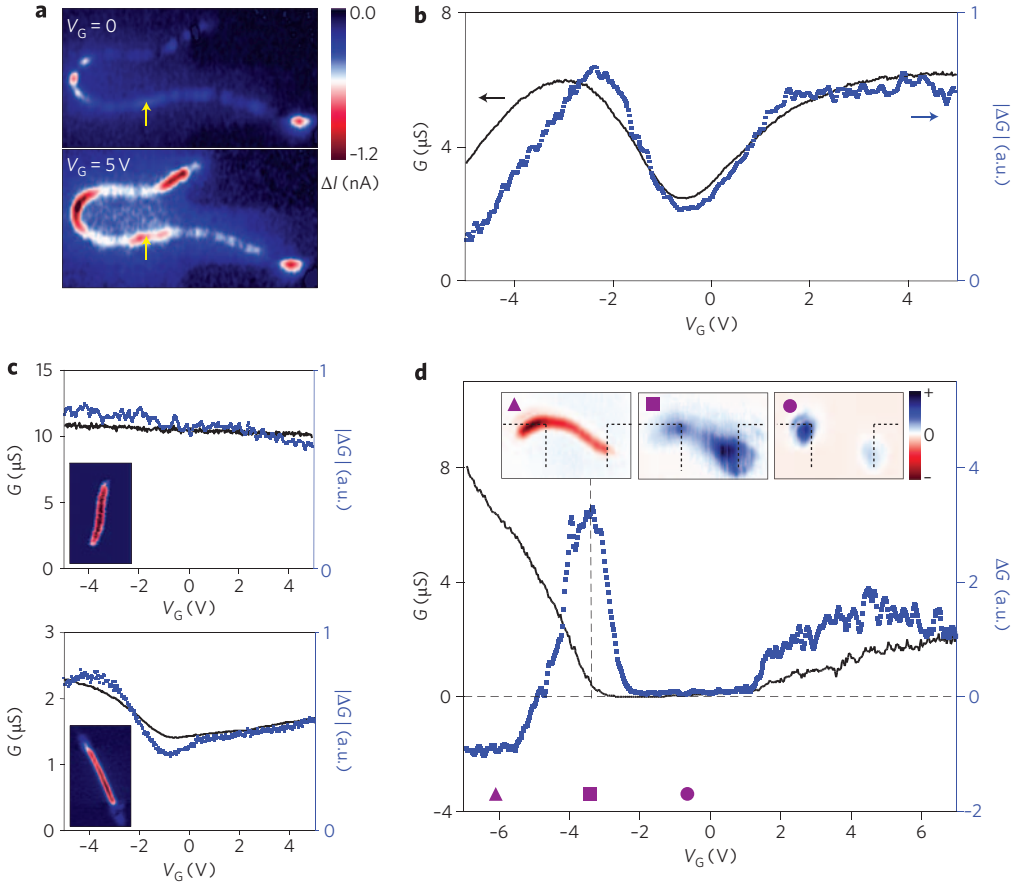

Figure 3 | Gate dependence of photothermal current. a, PTCM images of semi-metallic device D1 with $V_D = 0.2$ V, $V_G = 0$ and 5 V taken with standard lock-in. The overall signal is larger for $V_G = 5$ V, indicating that the nanotube is more conductive at that bias. **b**, $|\Delta G|$ (blue dots), measured with the laser fixed on the arrow shown in **a**, and G (black line, measured simultaneously) versus V_G. A close correspondence is observed between the two signals. **c**, ΔG and G versus V_G for metallic and semi-metallic carbon nanotube devices D5 (top) and D6 (bottom). Again, the two signals track closely. Insets: PTCM images of each device. **d**, ΔG and G versus V_G for semiconducting device D7 shows conductance enhancement close to turn-off. Insets: Photothermal current images at different values of gate bias (indicated by corresponding markers), tuned to turn the device on (left) and off (right). Between these two states, conductance enhancement (middle) is observed.

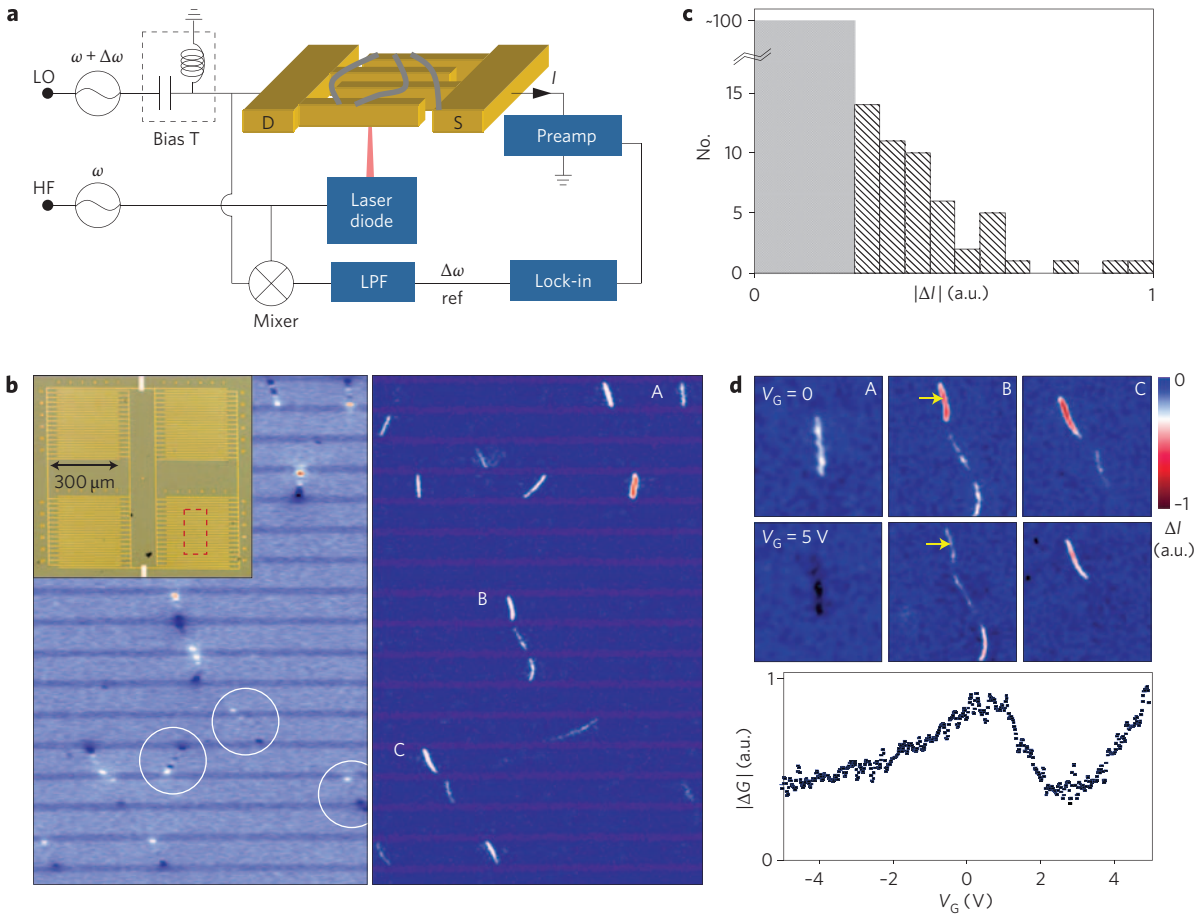

Figure 4 | PTCM on large-scale carbon nanotube transistors. a, Schematic of the heterodyne detection setup and the large-scale nanotube device under study. We modulate both the laser and source–drain bias, and detect the current signal through the lock-in at the difference frequency obtained by using a mixer followed by a low-pass filter (LPF). A d.c. grounded bias-T is used at the drain to reduce low-frequency noise. **b**, Inset: optical image of the large-scale carbon nanotube transistor L1. The device consists of two interdigitated electrodes on top of hundreds of randomly grown carbon nanotubes. Each quadrant measures ~300 × 300 μm. Right: PTCM image of the area outlined in red on L1 taken using the heterodyne detection setup with $V_G = 0$. Left: photocurrent image ($V_D = 0$) of the same scan area. The circled photocurrent spots are from nanotubes with no visible photothermal current and are most likely poorly conducting. **c**, Distribution of photothermal current intensities for over 150 carbon nanotubes from large-area scans. The large bar denotes low-conductance nanotubes without visible photothermal current, but which are confirmed to exist through photocurrent scans. This plot should scale with the absolute conductance of the nanotubes. **d**, Top: PTCM images of nanotubes A, B and C from **b** at $V_G = 0$ and 5 V. Different nanotubes and nanotube segments respond differently to the gate. Bottom: $|\Delta G|$ measured with the laser parked on the arrow on nanotube B versus V_G.

we now also show how we can study the gate dependence of the electrical conductance of individual metallic and semiconducting nanotubes.

In Fig. 3a we show PTCM images of semi-metallic nanotube D1 at two different gate biases $V_G = 0$ and 5 V ($V_D = 0.2$ V, standard lock-in). The overall current signal is clearly much stronger at $V_G = 5$ V, suggesting that the nanotube becomes more conductive there. To study this behaviour more quantitatively, as well as to eliminate gate hysteretic effects[19], we scanned the laser at a fixed location along the nanotube and measured photothermal current (heterodyne) simultaneously with G while continuously varying V_G. In Fig. 3b, we plot $|\Delta G|$ (blue dots) and G (black solid line) as a function of V_G. We see that the two quantities track closely for all values of V_G. The odd dip in the transport curve at $V_G < -3$ V could be due to defects more prevalent at these nanotube lengths[20]. For all metallic and semi-metallic devices measured to date (approximately 10), we observe a close correspondence between the gate dependences of ΔG and G. In Fig. 3c, we show similar plots for devices D5 and D6, which exhibit this correspondence at all gate biases. Their PTCM images are shown in the insets.

We have also performed the same measurements on an individual semiconducting nanotube device D7 with a well-defined bandgap (Fig. 3d). We see that the laser induces photothermal current when the transistor is in the 'on' state at negative V_G (left inset), but it apparently disappears altogether in the nanotube body once the device is 'off' (right inset, see Supplementary Information, Fig. S4). Conductance is, however, enhanced upon laser illumination when V_G is tuned between the two regimes (middle inset). This conductance enhancement, which is strongest near the conductance turn-off (see the blue curve in the main panel), is probably due to a laser-induced thermal excitation of additional carriers[13]; however, further experiments will be necessary to examine additional effects, such as photoconductivity[12] and photoelectric gating[12,13].

Unlike traditional transport measurements, PTCM is not limited to addressing only individually contacted devices, because each conducting pathway can produce photothermal current upon laser illumination. In fact, devices with more than one nanotube can be synthesized more easily with random growth and large electrode geometry; our heterodyne technique (Fig. 4a) can provide spatially resolved conductance information on single nanotubes in such devices.

The inset of Fig. 4b shows an optical image of a large-scale nanotube device L1 with two interdigitated electrodes that lie on top of randomly grown nanotubes. Each quadrant has dimensions of ~300 × 300 μm, and the entire device consists of hundreds of nanotubes. On the right of Fig. 4b we show a PTCM image of the area outlined in red on L1, taken with heterodyne detection ($V_G = 0$). We note that because such multi-nanotube devices have a much higher noise floor, we can detect their current signals using only this high-frequency detection scheme. The reflection image is again overlaid so that the electrodes are visible. We can clearly see the photothermal current from many nanotubes, with the strength of each signal reflecting the measure of conductance of each nanotube. An SPC image ($V_D = 0$) of the same scan area is shown on the left for comparison. Although photocurrent is universally visible for most nanotubes, allowing us to locate contacted nanotubes regardless of their conductance, photothermal current will be stronger for more conductive nanotubes. Indeed, most nanotubes can be seen in both images, but several that have clear photocurrent spots (circled in white) do not show visible photothermal current. We expect that these particular nanotubes are poorly conducting at this gate bias, and so their current signals are hidden within the noise floor.

Using this scheme, we can qualitatively determine the relative conductance distribution for a large number of nanotubes. In Fig. 4c, we show a histogram of the photothermal current observed for over 150 nanotubes from large area scans. The large bar at the far left denotes low-conductance nanotubes that are not resolved from PTCM imaging yet are confirmed to exist through SPC scans. From our previous analysis, we believe that this plot should scale closely with the nanotubes' absolute conductances, although a more detailed study will be required to develop a technique with better quantitative information.

It is also possible to determine the gate-dependent conductance behaviour of individual nanotubes in this array geometry by studying how their photothermal current changes with V_G. In Fig. 4d (top) we show small-area scans of nanotubes A, B and C from Fig. 4b at $V_G = 0$ and 5 V, and we can see how each nanotube responds differently to the gate. In particular, nanotube A disappears at $V_G = 5$ V, indicating that it is a semiconducting nanotube. We also see that different segments of nanotubes B and C contacting different electrodes behave distinctly. To obtain more quantitative information, one can fix the laser on individual nanotube segments and measure the photothermal current (or ΔG) while continuously varying V_G (as shown in the bottom of Fig. 4d for the top segment of nanotube B).

In conclusion, we have demonstrated a nanotube conductance imaging technique based on the linear relationship between photothermal current induced by optical heating and the overall nanotube conductance. We expect that the use of a tuneable laser with PTCM will allow for direct absorption spectroscopy of carbon nanotubes. Furthermore, PTCM should be applicable to other linear nanostructures as well, including semiconducting nanowires[21], graphene nanoribbons[22] and nanofabricated conducting polymers.

Methods

Device fabrication. Our carbon nanotube devices were fabricated using standard photolithography techniques with CVD-grown nanotubes. Nanotubes were synthesized from both patterned and randomly deposited catalysts on top of a 300-nm-thick layer of thermal oxide. Metal evaporation and lift-off were used to define source and drain electrodes (5 nm/45 nm chromium/gold or 20 nm/1.6 nm/35 nm palladium/chromium/gold), and the underlying silicon substrate was used as a global backgate.

Experimental setup. In our setup, we focused a ~1 mW laser beam ($\lambda = 658$ nm) using a microscope objective (NA = 0.7) onto a 1 μm full-width at half-maximum diffraction-limited spot (intensity ~1×10^5 W cm^{-2}) near our biased nanotube transistor. As a scanning mirror galvo rastered the beam across the sample at a rate of 5–20 Hz in the fast scanning direction, we recorded the electrical current flowing through the device as a function of the position of the laser spot. We also measured the intensity of the reflected light to determine the absolute position of the beam. To improve the signal-to-noise ratio of the current signal, we electrically modulated the laser diode so that the light output was sinusoidal, with minimum intensity very close to zero, and we detected the a.c. current in phase with the d.c. current using lock-in.

Two different detection schemes were used in this experiment. In standard lock-in detection (Fig. 1a), the laser was modulated at a frequency of 20 kHz, the source–drain bias V_D held constant, and current was measured at the laser modulation frequency. In heterodyne detection (Fig. 4a), both the laser and V_D were modulated close to 11 MHz, and the current measured at the difference frequency of 8 kHz. Details of this technique can be found in the work of Sazonova and colleagues[23]. The heterodyne technique is preferred for large-scale transistors, because a fixed d.c. bias required for the standard lock-in technique will generate a d.c. current that is so large that we would no longer be able to detect the nanotubes' photothermal current signals amid the current noise. An a.c. modulation of V_D eliminated the large d.c. current in our device and improved the signal-to-noise ratio dramatically. A d.c. grounded bias-T was used at the drain to further eliminate unwanted low-frequency noise (see Supplementary Information for comparison of the two detection methods).

All measurements were conducted in the ambient condition (room temperature and air environment).

Other possibilities for light-induced conductance decrease. We ruled out photoelectric gating[12,13] or other surface effects that originate from the exterior of the nanotube as the cause for the observed conductance decrease for two reasons. First, a line cross-section of the current signal in Fig. 1b was closely fitted to a Gaussian with a width equal to the diffraction-limited linewidth of our focused laser. Any photoelectric gating effect from the silicon substrate would have enlarged the signal width due to the presence of the 300-nm gate oxide. Furthermore, the laser polarization dependence of the current signal (Fig. 1c, middle; $V_D = 0.2$ V, standard lock-in) revealed that $|\Delta I|$ is maximum (minimum) when the incident light is polarized parallel (perpendicular) to the axis of the nanotube, proving unambiguously that the observed signal is attributable to light absorption by the nanotube itself[12]. Quite consistently, the image in Fig. 1b shows stronger signal in segments where the nanotube is parallel to laser polarization.

Molecular photodesorption[14] also cannot explain the conductance decrease because this process occurs on a timescale of several seconds, whereas our current signal shows no appreciable change from d.c. up to 20 kHz laser modulation (standard lock-in). Furthermore, the fact that the observed effect is quite insensitive to growth and fabrication processes makes photodesorption an unlikely candidate from the outset.

Estimate of ΔT. The average temperature increase ΔT in the nanotube was determined from the light power absorbed and thermal diffusion. Although we do expect a strong wavelength dependence for light absorption in semiconducting nanotubes around the E^S_{11} resonance[24], their higher energy E^S_{22} resonances as well as the E^M_{11} resonances for metallic nanotubes were shown to be broader with more modest on/off resonance ratios. This is further corroborated by work by Islam and colleagues on nanotube ensembles with a narrow diameter distribution[15], which shows relatively uniform spectral dependence above E^M_{11}.

For almost all of our devices measured (diameter > 2 nm), the $\lambda = 658$ nm (1.88 eV) laser energy was above all of the aforementioned resonances[25] for single-walled nanotubes, so we suspect that any spectral dependence in their photothermal current will be relatively modest. To support this, we performed the same PTCM measurements using a $\lambda = 410$ nm (3.02 eV) laser on five of the eleven nanotube devices measured in Fig. 2b (main panel). When we compare the results with those obtained for the $\lambda = 658$ nm laser of equal intensity (Fig. 2b, inset), we observe little difference between these two wavelengths, consistent with our claim as well as the results of Islam and colleagues[15].

The situation is more complicated if these devices consisted of multiwalled nanotubes or nanotube bundles. Although their precise spectral dependence is unknown due to the lack of published work on the subject, our laser energy is still far above the E^S_{11} resonance.

The lack of strong spectral dependence then suggests a simple linear relationship between light absorption and the nanotube diameter d. Also, for long (>~0.5 μm) nanotubes on silicon oxide, the heat gained from the laser is lost primarily through diffusion through the supporting substrate[26], and so we expect thermal conductance between the nanotube and the substrate to increase linearly with d. The overall dependence on d then cancels, giving us similar ΔT for nanotubes of different diameter, but similar lengths. From our data, we extract $\Delta T = 0.4$ K on average per 1 mW laser illumination for ~5-μm-long nanotubes.

Received 16 September 2008; accepted 6 November 2008; published online 14 December 2008

References

1. Saito, R., Dresselhaus, G. & Dresselhaus, M. S. *Physical Properties of Carbon Nanotubes* (Imperial College Press, 1998).
2. Jorio, A. *et al.* Carbon nanotube photophysics. *Mater. Res. Soc. Bull.* **29,** 276–280 (2004).

3. McEuen, P. L. & Park, J. Y. Electron transport in single-walled carbon nanotubes. *Mater. Res. Soc. Bull.* **29,** 272–275 (2004).
4. Avouris, P. Carbon nanotube electronics and optoelectronics. *Mater. Res. Soc. Bull.* **29,** 403–410 (2004).
5. Itkis, M. E., Borondics, F., Yu, A. P. & Haddon, R. C. Bolometric infrared photoresponse of suspended single-walled carbon nanotube films. *Science* **312,** 413–416 (2006).
6. Balasubramanian, K. *et al.* Photoelectronic transport imaging of individual semiconducting carbon nanotubes. *Appl. Phys. Lett.* **84,** 2400–2402 (2004).
7. Lee, E. J. H. *et al.* Electronic-band-structure mapping of nanotube transistors by scanning photocurrent microscopy. *Small* **3,** 2038–2042 (2007).
8. Freitag, M. *et al.* Imaging of the Schottky barriers and charge depletion in carbon nanotube transistors. *Nano Lett.* **7,** 2037–2042 (2007).
9. Ahn, Y. H., Tsen, A. W., Kim, B., Park, Y. W. & Park, J. Photocurrent imaging of p–n junctions in ambipolar carbon nanotube transistors. *Nano Lett.* **7,** 3320–3323 (2007).
10. Purewal, M. S. *et al.* Scaling of resistance and electron mean free path of single-walled carbon nanotubes. *Phys. Rev. Lett.* **98,** 186808 (2007).
11. Zhou, X., Park, J. Y., Huang, S., Liu, J. & McEuen, P. L. Band structure, phonon scattering and the performance limit of single-walled carbon nanotube transistors. *Phys. Rev. Lett.* **95,** 146805 (2005).
12. Freitag, M., Martin, Y., Misewich, J. A., Martel, R. & Avouris, P. H. Photoconductivity of single carbon nanotubes. *Nano Lett.* **3,** 1067–1071 (2003).
13. Pankove, J. I. *Optical Processes in Semiconductors* (Dover Publications, 1975).
14. Chen, R. J. *et al.* Molecular photodesorption from single-walled carbon nanotubes. *Appl. Phys. Lett.* **79,** 2258–2260 (2001).
15. Islam, M. F., Milkie, D. E., Kane, C. L., Yodh, A. G. & Kikkawa, J. M. Direct measurement of the polarized optical absorption cross-section of single-wall carbon nanotubes. *Phys. Rev. Lett.* **93,** 037404 (2004).
16. Lauret, J. S. *et al.* Ultrafast carrier dynamics in single-wall carbon nanotubes. *Phys. Rev. Lett.* **90,** 057404 (2003).
17. Wang, F., Dukovic, G., Brus, L. E. & Heinz, T. F. Time-resolved fluorescence of carbon nanotubes and its implication for radiative lifetimes. *Phys. Rev. Lett.* **92,** 177401 (2004).
18. Maune, H., Chiu, H. Y. & Bockrath, M. Thermal resistance of the nanoscale constrictions between carbon nanotubes and solid substrates. *Appl. Phys. Lett.* **89,** 013109 (2006).
19. Lee, J. S. *et al.* Origin of gate hysteresis in carbon nanotube field-effect transistors. *J. Phys. Chem. C* **111,** 12504–12507 (2007).
20. Bockrath, M. *et al.* Resonant electron scattering by defects in single-walled carbon nanotubes. *Science* **291,** 283–285 (2001).
21. Lieber, C. M. Nanoscale science and technology: Building a big future from small things. *Mater. Res. Soc. Bull.* **28,** 486–491 (2003).
22. Obradovic, B. *et al.* Analysis of graphene nanoribbons as a channel material for field-effect transistors. *Appl. Phys. Lett.* **88,** 142102 (2006).
23. Sazonova, V. *et al.* A tunable carbon nanotube electromechanical oscillator. *Nature* **431,** 284–287 (2004).
24. Berciaud, S., Cognet, L., Poulin, P., Weisman, R. B. & Lounis, B. Absorption spectroscopy of individual single-walled carbon nanotubes. *Nano Lett.* **7,** 1203–1207 (2007).
25. Dresselhaus, M. S., Dresselhaus, G., Saito, R. & Jorio, A. Raman spectroscopy of carbon nanotubes. *Phys. Rep.* **409,** 47–99 (2005).
26. Pop, E. The role of electrical and thermal contact resistance for Joule breakdown of single-wall carbon nanotubes. *Nanotechnology* **19,** 295202 (2008).

Acknowledgements

The authors thank N. M. Gabor and P. L. McEuen for helpful discussions. This work was supported by a grant from the Air Force Office of Scientific Research (FA9550-07-1-0338) and the National Science Foundation (NSF) CAREER grant (DMR-0748530). Sample fabrication was performed at the Cornell Nano-Scale Science and Technology Facility as well as at the Harvard Center for Nanoscale Systems' Nanofabrication Facility.

Author contributions

A.W.T and J.P conceived the experiments, J.P designed the experimental apparatus and A.W.T performed the experiments and analysed the data with J.P. A.W.T., H.K. and L.A.K.D. fabricated the devices, and L.H.H. aided with the experiments. A.W.T. and J.P. co-wrote the paper. All authors discussed the results and commented on the manuscript.

Additional information

Supplementary Information accompanies this paper at www.nature.com/naturenanotechnology. Reprints and permission information is available online at http://npg.nature.com/reprintsandpermissions/. Correspondence and requests for materials should be addressed to J.P.